PAPER • OPEN ACCESS

Absolute nuclear charge radius by Na-like spectral line separation in high-Z elements

To cite this article: A Hosier *et al* 2024 *J. Phys. B: At. Mol. Opt. Phys.* **57** 195001

View the article online for updates and enhancements.

Absolute nuclear charge radius by Na-like spectral line separation in high-Z elements

A Hosier[1,2,*] , **Dipti**[3] , **S A Blundell**[4], **R Silwal**[5] , **A Lapierre**[6], **J D Gillaspy**[2,8], **G Gwinner**[9] , **J N Tan**[7], **A A Kwiatkowski**[10,11], **Y Wang**[10,12], **H Staiger**[1,2], **A C C Villari**[6], **Yu Ralchenko**[7] **and E Takacs**[1,2]

[1] Department of Physics and Astronomy, Clemson University, Clemson, SC 29634-0978, United States of America
[2] Associate, National Institute of Standards and Technology, Gaithersburg, MD 20899, United States of America
[3] International Atomic Energy Agency, Vienna A-1400, Austria
[4] University of Grenoble Alpes, CEA, CNRS, IRIG, SyMMES 38000 Grenoble, France
[5] Department of Physics and Astronomy, Appalachian State University, Boone, NC 28608, United States of America
[6] Facility for Rare Isotope Beams, East Lansing, MI 48824, United States of America
[7] National Institute of Standards and Technology, Gaithersburg, MD 20899, United States of America
[8] National Science Foundation, Alexandria, VA 22314, United States of America
[9] Department of Physics and Astronomy, University of Manitoba, Winnipeg MB R3T 2N2, Canada
[10] TRIUMF, Vancouver, BC V6T 2A3, Canada
[11] Department of Physics and Astronomy, University of Victoria, Victoria, BC V8P 5C2, Canada
[12] Department of Physics and Astronomy, University of British Columbia, Vancouver, BC V6T 1Z4, Canada

E-mail: ahosier@clemson.edu

CrossMark

Abstract

We describe a novel technique to determine absolute nuclear radii of high-Z nuclides. Utilizing accurate theoretical atomic structure calculations together with precise measurements of extreme ultraviolet transitions in highly charged ions this method allows for precise determinations of absolute nuclear charge radii based upon the well-known nuclear radii of their neighboring elements. This method can work for elements without stable isotopes, and its accuracy may be competitive with current methods (electron scattering and muonic x-ray spectroscopy).

---

* Author to whom any correspondence should be addressed.

J. Phys. B: At. Mol. Opt. Phys. **57** (2024) 195001

A Hosier *et al*

1. Introduction to nuclear charge radius measurements

The distribution of charge and its radius in an atomic nucleus are some of the most studied fundamental properties of the atom since the days of Rutherford. An accurate determination of these properties and knowledge of how they evolve across the periodic table and isotopic chains are a major interest in nuclear physics, atomic physics, and searches for physics beyond the Standard Model (see e.g. [1–3]). The nuclear charge radius is typically reported as the root mean square (RMS) $\langle r^2 \rangle^{1/2}$ of the charge distribution [4].

1.1. Absolute RMS charge radii and their determination

One of the conventional methods that allows for absolute nuclear charge radius measurements in high-Z elements is muonic x-ray spectroscopy [5–7]. This method investigates the energy levels of an orbiting muon captured by an atomic system to form an exotic atom. Measured low-lying hydrogen-like transition energies are compared to accurate muonic-atomic structure calculations based on an assumed charge distribution, such as a Fermi distribution, and other parameters (e.g. deformation factors). Due to the large mass of the muon, which is 207 times heavier than the electron, the muon and nuclear wavefunctions strongly overlap making muonic atoms a very sensitive system to probe the nucleus in comparison to normal atoms with electrons. The most difficult component that needs to be treated in their theoretical analysis, and limits the accuracy of nuclear charge radii extracted from muonic atom spectroscopic measurement, is the nuclear polarization correction, which is nuclear-structure dependent. It originates from the electromagnetic interaction between the muon and nucleus exciting the system into virtual states resulting in a shift of the muon binding energies. This correction can be evaluated from different theoretical approaches [8]. Due to inadequate knowledge of nuclear-excited states, the uncertainty of the calculation of the nuclear polarization limits the accuracy of the method. Despite that, charge-radius values with a relative accuracy as low as 0.02% can be obtained for spherical nuclei such as ^{208}Pb.

Another conventional method for measuring absolute nuclear charge radii in high-Z elements is elastic electron scattering [6, 8–10]. This method consists of observing scattered electrons giving insight into the underlying charge distribution from a model-independent approach [11]. In using elastic electron scattering, the measured quantity is the differential cross section for high-energy electrons scattering through an angle from a target detected within a solid angle. In non-relativistic (spin-less) scattering theory and within the framework of the first Born approximation, the incoming electron beam can be represented as a plane wave. The outgoing spherical waves are created at all points of the scattering potential. The differential cross section can then be described as the product of a point-like scattering cross section and the square of a form factor, which is the Fourier transform of the charge distribution. Nuclei and electrons have spins leading to more complex form factors which can be interpreted as electric and magnetic distributions in the relativistic theory. In both theories, the charge radius can be obtained from the form factors in the limit of extrapolation of very low momentum transfer. This method can be affected by inelastic components, which have to be carefully excluded. Electron scattering allows for a determination of the radial charge distribution, unlike other methods which only provide integral quantities such as the RMS radius and higher moments of charge distribution.

Both, muonic x-ray spectroscopy and elastic electron scattering, have been extremely successful methods. They have provided the majority of the absolute nuclear charge radii measured in stable isotopes for over 5 decades. In addition to the need for producing sufficient quantities of muons and generating high-energy electrons, the necessity of macroscopic amounts of target material has limited their applicability to short-lived radioactive isotopes. However, recent developments have shown that muonic x-ray spectroscopy [13, 14] and elastic electron scattering can be performed with high precision on limited target quantities. In particular, the new SCRIT ion trap facility [15], dedicated to electron scattering on radioactive isotopes, expects to perform measurements on as low as 10^8 ions.

1.2. RMS charge radius differences

Apart from absolute nuclear charge radius determination, methods for relative difference measurements between isotopes of the same element are also available. A frequently utilized method is the K_α isotope shift [6, 12]. This method determines the difference in nuclear charge radii by measuring the isotope shift of an element in the K_α inner shell transitions. Another method is based on similar ideas, called an optical isotope shift [16, 17], which measures the isotope shift for a particular element using an optically accessible valence level transition.

In both of these main methods for nuclear charge radii differences, the shift in measured energy can be attributed to two main sources: the mass shift (MS, due to the difference in the nuclear masses in a set of isotopes) and the field shift (FS, due to the difference in nuclear charge distributions). These methods can provide highly precise experimental results with the major difficulty arising from the theoretical calculations of complex electronic structure and the need for approximations to include quantum electrodynamics (QED) effects [18].

1.3. Measurements involving highly charged ions

X-ray spectroscopy of few-electron uranium ions has been proven in the past to be sensitive to nuclear size, specifically to the mean square radius difference between ^{235}U and ^{238}U isotopes [20]. Other methods including dielectronic recombination have also been investigated for RMS nuclear charge determination using highly charged ions [21, 22], but neither of these methods gained major traction due to the scarcity of the charge states required to perform these studies [19]. Dielectronic recombination measurements of [22] used Li-like Nd by measuring the $2s - 2p_{1/2}$ and $2s - 2p_{3/2}$ transitions.
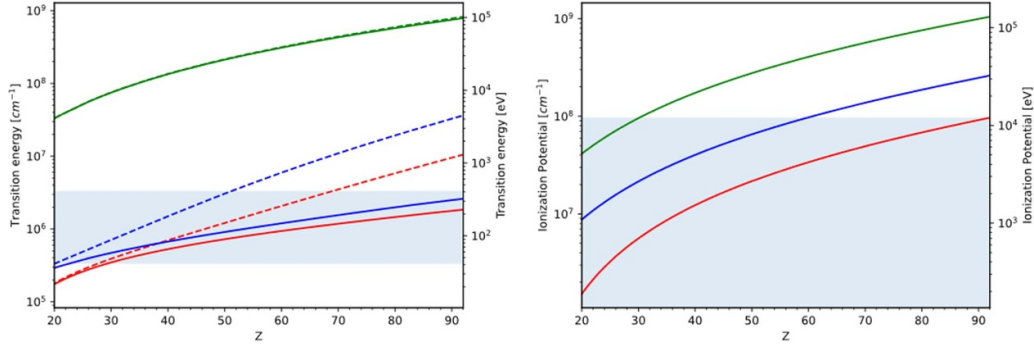
J. Phys. B: At. Mol. Opt. Phys. **57** (2024) 195001

A Hosier *et al*

Figure 1. (Left) Plot of transition energies from $Z = 20$ to $Z = 92$, with Na-like D1 $3s\,^2S_{1/2} \to 3p\,^2P_{1/2}$ [23] (red solid), Na-like D2 $3s\,^2S_{1/2} \to 3p\,^2P_{3/2}$ [23] (red dashed), Li-like $1s^2 2s\,^2S_{1/2} \to 1s^2 2p\,^2P_{1/2}$ [24] (blue solid), Li-like $1s^2 2s\,^2S_{1/2} \to 1s^2 2p\,^2P_{3/2}$ [24] (blue dashed), H-like $1s\,^2S_{1/2} \to 2p\,^2P_{1/2}$ [25] (green solid), and H-like $1s\,^2S_{1/2} \to 2p\,^2P_{3/2}$ [25] (green dashed). The shaded blue region indicates EUV range (3–30 nm). (Right) Plot of ionization potential necessary to create Na-like (red), Li-like (blue) and H-like (green) ions. The shaded blue region indicates the typical range of optimum electron beam energies used to generate highly charged ions [26]).

Comparison with QED calculations allowed to determine the isotope shift between ^{142}Nd and ^{150}Nd.

Recently, Silwal *et al* [27] demonstrated a new method for measuring the mean-square difference of nuclear charge radii of isotopes based on extreme-ultraviolet spectroscopy of Na-like highly charged ions. This method extracts nuclear radii by comparing accurate atomic structure calculations with the precise wavelengths measured for the ground state electric dipole transitions in Na-like charge states. The nuclear charge radii differences between ^{124}Xe and ^{136}Xe isotopes were determined in this first demonstration. An extension to this method was made in [28] by using other simple highly charged atomic systems such as Mg-like and Al-like to reduce the uncertainty in the mean-square difference of the nuclear charge radii of Xe isotopes reported in [27].

The choice for the charge states of ions was due to their highly calculable valence electron configurations (the transitions observed are located in an experimentally convenient portion of the electromagnetic spectrum) and the 3 s valence electron in highly charged ions has significant wavefunction overlap with the nucleus, making them excellent candidates for nuclear probes. Applying highly charged ions in isotope shift measurements allows for competitive mean-square differences in nuclear charge radii produced through optical and K_α isotope shift measurements.

1.4. Absolute measurement based on Na-like ions

The main idea behind the current proposal to use Na-like ions for determining absolute nuclear charge radii for isotopes of high-Z elements is to use a reference isotope with a well-known nuclear radius and extend the Na-like isotope shift method of [27, 28] to line shifts between nearby elements. By measuring the difference in Na-like D1 $3s\,^2S_{1/2} \to 3p\,^2P_{1/2}$ transition energies for these elements, and using highly accurate atomic structure theory to calculate the same difference, it is possible to determine the absolute nuclear charge radius of the second isotope.

Na-like systems are favorable from two different points of view for this measurement. The first is their highly calculable

electronic structure [23], similar to Li-like [29] and H-like [30], one-electron or quasi one-electron systems. Calculations for these atomic systems are highly accurate compared to their many-valence electron counterparts. From the energies of the main spectral lines in these systems, plotted in figure 1, one can see that the energies of the Na-like D1 transitions reside in the blue-shaded region, which is the easily accessible EUV range using precise standard spectroscopic methods. Li-like and H-like ions would further reduce theoretical uncertainties, however the production of these systems are difficult in current EBIT devices and the transition energies are in the x-ray range.

In the following, we introduce the major concepts and assumptions of this technique for absolute nuclear charge radius determination and will look into the main sources of uncertainties one needs to consider in carrying out such an experiment.

2. Concept of the measurement

Let us assume that a reference nuclide A has a literature-recommended nuclear charge radius of $R_A = \sqrt{\langle R^2 \rangle_A}$ with a small literature-recommended uncertainty ΔR_A (e.g. from [4]). Our goal is to determine the nuclear charge radius R_B of a nuclide B of interest with an uncertainty of ΔR_B by accurately measuring the separation of the Na-like D1 transition energies between the nuclides of A and B. One of the strengths of this technique is that the two Na-like ions can be isotopes of different elements as long as one can accurately measure the energy separation of the two lines, and accurate theoretical calculations are available for the sensitivity of the line energies on small changes of the nuclear radius.

For small nuclear radius-dependent changes we can assume that the change in the line energy is linearly dependent on the change in the nuclear charge radius, $\delta E \propto \delta R$. This assumption is based on the idea that for high-Z systems the theoretical energy shift is mainly determined by the field shift as $\delta E = F \delta \langle R^2 \rangle$, where F is the so-called field shift coefficient known from isotope shift determinations [27, 28]. If

the nuclear radius we choose for the calculations is close to the real value we are trying to determine from our measurement, then $\delta\langle R^2\rangle \equiv (R+\delta R)^2 - R^2$ can be approximated by $2R\delta R$, and the field shift coefficient by $F = S/(2R)$. This gives $\delta E = S\delta R$, expressing the linear proportionality between the two quantities.

S is the so-called nuclear sensitivity coefficient introduced before in [23] where Na-like D1 and D2 line energies have been compiled and calculated. By definition, the S nuclear sensitivity coefficient tells how much the transition energy changes with a slight δR change of the nuclear charge radius used in the calculations, typically in units of $\mathrm{cm}^{-1}\,\mathrm{fm}^{-1}$.

$$S \equiv \frac{E(R+\delta R) - E(R)}{\delta R}, \qquad \delta R \ll R. \qquad (1)$$

For nuclide B for which, based on our previous assumption, the nuclear charge radius is not as accurately known, the real energy $E_B(R_B)$ can be expressed as a first-order correction to a theoretical transition energy $E_B(R_{B0})$, calculated assuming a nuclear charge radius R_{B0}, the literature-recommended value for example from [4]. We note that the chosen value does not need to be any special number, the only importance is that it is close to the real value to be determined so that our linear approximations are valid. Hence

$$E_B(R_B) = E_B(R_{B0}) + S_B\delta R_B, \qquad (2)$$

where

$$\delta R_B = R_B - R_{B0}. \qquad (3)$$

Here, R_B is the true value that we intend to determine from the experiment. Since for nuclide A, the real value of the nuclear charge radius is assumed to be very close to the literature-recommended radius used in the atomic structure calculations ($R_A = R_{A0}$), in other words, R_A is accurately known, we can claim that

$$E_A(R_A) = E_A(R_{A0}). \qquad (4)$$

The difference between $E_B(R_B)$ and $E_A(R_A)$ is the experimentally measured difference of $E_{AB}^M \equiv E_B(R_B) - E_A(R_A)$, and with this

$$\delta R_B = \frac{1}{S_B}\left(E_{AB}^M + E_A(R_A) - E_B(R_{B0})\right). \qquad (5)$$

Here, δR_B represents the correction we need to make to the assumed R_{B0} nuclear charge radius for the calculated difference in the line energies to agree with the experimental measurement. The different theoretical and experimental contributions to its uncertainty determine the accuracy of the technique based on these ideas.

3. Atomic structure theories

One of the cornerstones of this method is the achievable accuracy of atomic structure calculations for Na-like
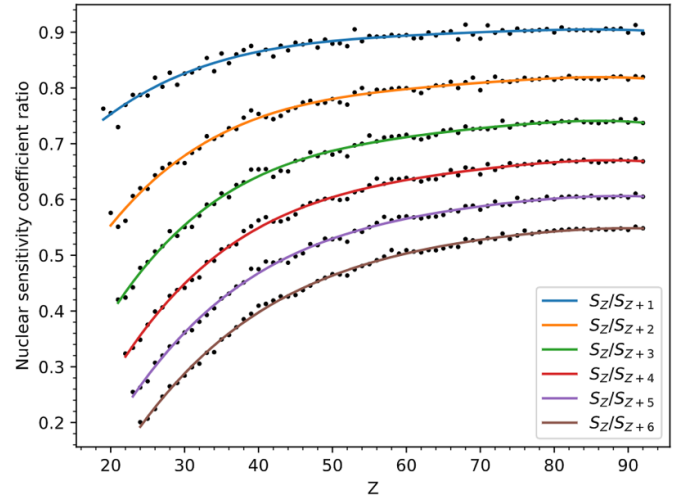

Figure 2. Nuclear sensitivity ratios of S_Z/S_{Z+N} where N ranges from 1 to 6 in this example to estimate the uncertainty contribution from the reference nuclide's RMS nuclear charge radius uncertainty. Nuclear sensitivity coefficient values are obtained from [23].

systems. Theoretical methods that have the required theoretical accuracy for evaluating Na-like systems are the relativistic many-body perturbation theory (RMBPT) with added quantum electrodynamic (QED) contributions [23, 31, 32], multi-configurational Dirac-Hartree-Fock method typically performed in the code GRASP [33], and the S-matrix formulation [34]. There are other sufficient methods, but here we will only discuss the three mentioned.

State-of-the-art Relativistic Many-Body Perturbation framework calculations have been performed in [31]. Their study focuses on calculating energies of 3 s, $3p_{1/2}$, and $3p_{3/2}$ states in Na-like ions with nuclear charges ranging from $Z = 11$ to 92. Employing relativistic many-body perturbation theory based on Dirac-Fock wave functions, the calculations include second- and third-order Coulomb correlation corrections, first-order corrections for transverse photon exchange, Breit interaction, as well as finite nuclear size, reduced mass, and mass-polarization corrections. Notably, QED corrections like electron self-energy and vacuum polarization are excluded but later included in follow-up publications [23, 32].

The multi-configuration Dirac-Hatree-Fock (MCDHF) method (e.g. [33]) is a universal relativistic approach to calculation of atomic wavefunctions that is based on a variational theory. Electron correlations are included by expanding the atomic state functions (ASF) in a linear combination of variationally determined configuration state functions (CSF) to describe the eigenfunctions of parity and angular momentum. The radial part of the one-electron orbitals and the expansion coefficients for CSFs are obtained in the relativistic self-consistent field procedure, and are normally followed by a relativistic configuration interaction calculation. The MCHDF applications typically include other relativistic (Breit) and QED corrections for multi-electron systems.

The S-matrix calculations for the Na-like isoelectronic sequence were reported in [34]. This fully relativistic QED-based method makes use of a modified Furry

representation with account of higher-order Feynmann diagrams and the Kohn–Sham potential used as a local potential for the Hamiltonian. In this approach, a complete description of the contribution to energy levels of all Feynman diagrams involving one and two photons is achieved, and the effects of three-photon exchanges are modeled by the third-order MBPT results. Additionally, one- and two-electron nuclear recoil corrections are included as well.

4. Experimental approach

One of the main experimental requirements for this method is the spectroscopy of highly ionized charge states of heavy elements in the Na-like isoelectronic sequence. There are several methods to produce low-density plasmas that can ionize high-Z elements to the desired Na-like isoelectronic sequence, such as electron beam ion traps (EBIT) and sources (EBIS), electron cyclotron resonances ion sources (ECRIS), accelerated beam based methods, tokamaks, and other laboratory plasma devices [36–39]. The electron beam ion trap is unique by providing the advantage of producing and trapping a narrow range of charge states [40], whereas other plasma sources can still provide charge states comparable to the EBIT but over a much broader range [41]. From here on, we will focus on the application of EBITs for this new type of measurement.

4.1. Electron beam ion trap

Due to its slit-like (narrow and long) plasma source, EBITs are especially suited for these measurements. Their highly tunable plasma environment allows for a precise selection of charge states across the periodic table. The EBIT is a small-scale laboratory device that utilizes a high-energy beam of electrons to ionize atomic species to desired charge states through electron-impact ionization and excite atomic transitions of ions of these charge states. Other interactions such as dielectronic recombination, radiative recombination, and charge exchange also occur inside the EBIT trap, contributing to the dynamic evolution of the charge state distribution and the observable transitions. With accelerating potentials for the electrons (reaching energies up to 30 kV in mid-scale EBIT devices), all of the Na-like charge states of the periodic table should be accessible in these devices. Figure 1 shows the ionization potentials of Mg-like charge states as a function of the nuclear charge necessary for producing Na-like ions of those elements. Further details about EBIT devices can be found in [42].

4.2. EUV spectroscopy of Na-like ions

The Na-like D1 transition, $3s\,^2S_{1/2} - 3p\,^2P_{1/2}$, lies in the extreme ultra-violet (EUV) range, see figure 1 for high-Z elements. High-resolution spectroscopic techniques are readily available for these wavelengths, and the investigation of the EUV region has produced many publications by the EBIT community [23, 43–45].

The flat field grazing incidence EUV spectrometer at NIST for example is ideally suited for the detection of Na-like D1

lines in the high-Z region of our current interest and therefore can serve as a good example to explore the different experimental considerations and the uncertainties to be taken into account in designing future nuclear charge radii measurements. Blagojevic *et al* [46] gave a detailed description of the design of the highly efficient EUV spectrometer at NIST, which includes a parabolic mirror to increase the solid angle of the detection.

The detector of choice for the National Institute of Standards and Technology (NIST) instrument is a back-illuminated liquid nitrogen-cooled charge-coupled device (CCD), which has an array of 512×2048 pixels with 13.6 micrometer $\times$ 13.6 micrometer size each, which is generally the state-of-the-art in this instrumentation (figure 2). The spatial dimensions of a pixel are an important consideration in these measurements because to be sensitive to the nuclear charge radii affected shift, the line separations are expected to be determined to a fraction of a pixel precision. In the case of Roshani *et al* [28], for example, the measured isotope shift was about a hundredth of a pixel. D1 line shifts of neighboring elements extend to several pixels, but the requirements for experimental precision are similar to the isotope shift determinations.

Because of the larger line separation, the precise calibration of these instruments becomes highly important. The calibration function for the NIST device is generally well approximated by a third-order polynomial [47–49], where the coefficients of this calibration polynomial can be found through least-squares minimization. The dependent variables in the fitting are assigned to the known wavelengths of the calibration lines with their small literature uncertainty. The independent variable is the line center found through standard curve fitting with an appropriate peak-like function. It can be for example a Gaussian if instrumental width is the limiting factor with the associated statistical uncertainty from the curve fitting procedure.

The one-σ confidence band of the calibration polynomial is generally referred to as the *calibration uncertainty* of the measurement at every particular wavelength and is associated with the covariance matrix of the fitted parameters of the calibration function. An additional source of potential uncertainty, denoted as the *systematic uncertainty*, should also be considered to be added as a scalar value in quadrature to all dependent variable uncertainties. The source and value of the systematic uncertainty are generally difficult to determine, and an often-used procedure is an iteration with a gradually increased value until the condition of $\chi^2_{\text{reduced}} = 1$ is satisfied for the calibration polynomial fit.

5. Considerations about the attainable accuracy

From equation (5), the uncertainty of the measured correction δR_B to the nuclear charge radius with respect to the theoretically assumed one can be expressed as

$$\Delta\left(\delta R_B\right)$$
$$= \sqrt{\frac{(S_A \Delta R_A)^2}{S_B^2} + \frac{\left(|\Delta\left[E_A\left(R_{A0}\right) - E_B\left(R_{B0}\right)\right]|\right)^2}{S_B^2} + \frac{(\Delta E_{AB}^M)^2}{S_B^2} + (\delta R_B)^2 \left(\frac{\Delta S_B}{S_B}\right)^2},$$

(6)

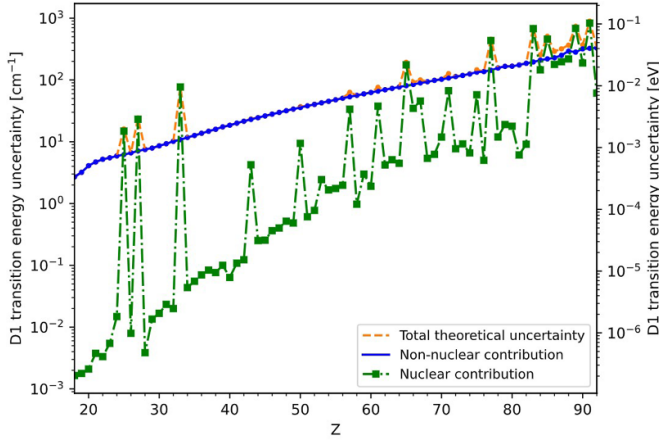J. Phys. B: At. Mol. Opt. Phys. **57** (2024) 195001

A Hosier *et al*

Figure 3. Theoretical uncertainty from nuclear and non-nuclear (including QED effects) contributions in a set of RMBPT calculations of the Na-like isoelectronic sequence [23]. Corrections to transition energies and uncertainties were made using up-to-date nuclear data [4] and natural isotope abundance ratios [35].

which has 4 main contributions, discussed in the next four sections.

5.1. Uncertainty of the reference element A nuclear charge radius

The first contribution is due to the uncertainty ΔR_A in the nuclear charge radius of the reference nuclide *A*. This contribution comes from using a reference nuclide's well-known absolute nuclear charge radius to extract an improved absolute value for the measured element, ultimately limiting the extracted uncertainty. The nuclear sensitivity coefficient for an element of atomic number *Z* can be estimated with a polynomial fit (equation (10)) of the nuclear sensitivity coefficients as a function of *Z* using the values tabulated in [23]. The ratio of the nuclear sensitivity coefficients between the reference nuclide and measured nuclide can be seen in figure 3.

5.2. Uncertainty of the difference of theoretical transition energies

The second term in equation (6) involves the uncertainty in the difference of theoretical transition energies. Note that the uncertainty here is $\Delta[E_A(R_{A0}) - E_B(R_{B0})]$, which is the theoretical uncertainty assuming the nuclear sizes have the values R_{A0} and R_{B0} used in the calculation. Now, the non-nuclear-size contribution to the atomic structure calculations for the transition energies is a smooth function of *Z*, and if one controls the purely numerical errors in the calculation to be negligible, the dominant uncertainty in the non-nuclear-size contribution arises from the omitted many-body and QED terms, which are also a smooth function of *Z*. (Apart from the nuclear size effect, the nuclear terms also include the nuclear recoil or mass effect, which in principle introduces small irregularities

as a function of *Z*, but is a very small effect.) Therefore, this theoretical uncertainty term should be treated like a systematic uncertainty and taken to be equal to the difference of the individual non-nuclear uncertainties, $\Delta[E_A(R_{A0}) - E_B(R_{B0})] = \Delta E_A(R_{A0}) - \Delta E_B(R_{B0})$. Using this approach to the theoretical uncertainty, rather than adding the individual theoretical errors $\Delta E_A(R_{A0})$ and $\Delta E_B(R_{B0})$ in quadrature, gives an overall reduction of the theoretical contributions to the uncertainty, which is ultimately limited by the uncertainty in the reference nuclear charge radius and experimental difference uncertainty. The nuclear and non-nuclear theoretical uncertainties, as estimated in [23], can be seen in figure 4 for the D1 transition as a function of *Z*. The uncertainty in hyperfine structure should be evaluated explicitly in this term as well.

5.3. Uncertainty of the difference in experimentally determined transition energies

This contribution comes from the uncertainty in the experimentally determined difference of transition energies. It includes statistical and calibration uncertainties with the latter generally also including a systematic uncertainty component. The statistical and calibration uncertainties are determined by the number of collected photons used to extract the line centers of the Na-like transitions and calibration lines respectively, along with the instrumental resolution σ at the energy of the measured or calibration line. Details of the uncertainty components of the measurements and the preferable methods to experimentally determine the energy separations are included in the appendix (section A). Contributions in the experimental uncertainty are added in quadrature.

5.4. Relative uncertainty of the nuclear sensitivity coefficient of the element to be measured

The final contribution is due to uncertainty in the nuclear sensitivity coefficient, which stems principally from the nuclear-model dependence. Suppose one considers the fluctuations in the change of transition energy $\delta E_B = S_B \delta R_B$, for constant δR_B, given by a large set of possible changes in the nuclear charge density, which is not necessarily assumed to be a uniform sphere, but can also include density changes localized around the nuclear surface or related to nuclear deformations, for example. By doing this, we find fluctuations in the inferred value of S_B at the few percent level. As an approximate rule, these fluctuations can be taken to be approximately one-half the total effect of the higher nuclear moments $\delta\langle r^4 \rangle$ and $\delta\langle r^6 \rangle$ in the Seltzer moment [50] for $Z \geqslant 60$. This uncertainty also contains estimations on uncertainties due to deformation, and nuclear polarization based on previous studies of Li-like ions. The final uncertainty of the extracted nuclear charge radius correction should use the proper tabulated values given in [23] or other theoretical works and the most up-to-date atomic and nuclear data [4] and not those given in the polynomial fit listed in this article.
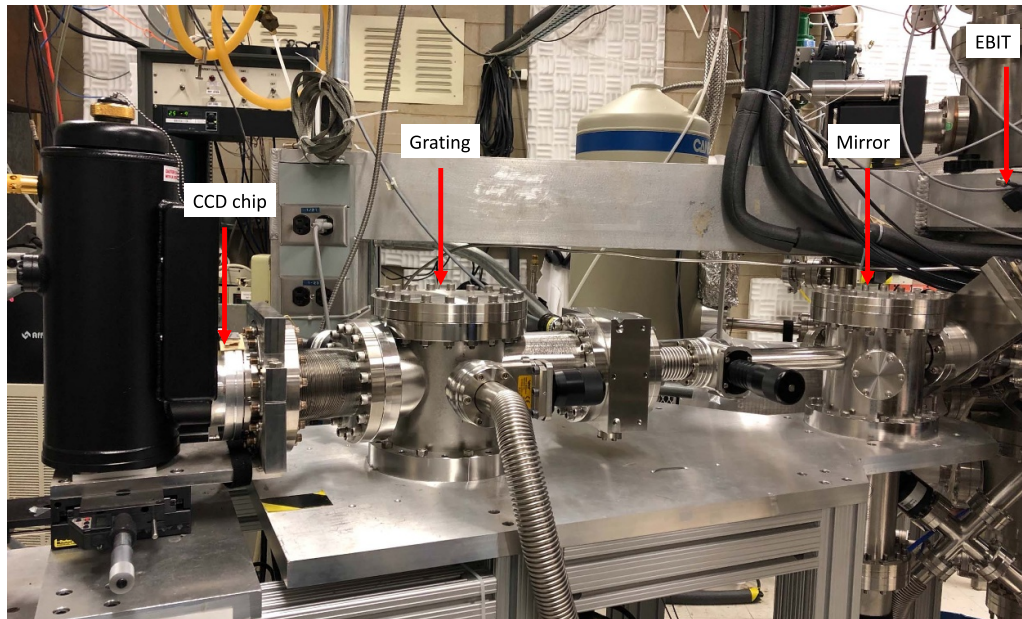
Figure 4. EUV spectrometer setup at the NIST EBIT.

6. Summary

Currently, there exist only a handful of methods for absolute nuclear charge radius determination which have been extensively explored in the last few decades. These methods, while shown to be successful where applicable, have various limitations. We introduce a new method for determining the absolute nuclear charge radii of high-Z elements based on standard spectroscopy methods of atomic physics combined with highly accurate atomic structure calculations. This new method has the ability to be applied to two different nuclides, providing flexibility with the choice of reference element based on available nuclear data and availability of the nuclide. With these estimations, it is evident that the achievable uncertainties of this method have the potential to be sensitive enough to support tests of physics beyond the Standard Model with isotopes that currently have no measured absolute nuclear charge radius. Other simple electronic systems such as Mg-like and Al-like can also be used given their transitions lie in the EUV spectroscopic region, and their uncertainties in electronic structure calculations are competitive with Na-like as discussed here.

Data availability statement

No new data were created or analysed in this study.

Appendix

A.1. Determining ΔE^M_{AB} experimental D1 separation uncertainty

There are two approaches that allow the determination of the E^M_{AB} energy separation of the D1 lines of interest. The precise measurement of the absolute positions of both lines and taking the difference or the measurement of the separation directly. The choice between the two approaches depends on the separation of the two D1 lines and the precision of the calibration one can achieve in an experiment.

The energy separation to first order depends on atomic number, so for nuclides of the same or neighboring elements the separation could be small. In this case the uncertainty that comes from measuring the D1 line separation by subtraction of the absolute energy positions, $E^M_{AB} = E^M_B - E^M_A$, carry several uncertainty components

$$\Delta E^M_{AB} = \sqrt{\Delta E^2_{A,\text{stat}} + \Delta E^2_{A,\text{cal}} + \Delta E^2_{B,\text{stat}} + \Delta E^2_{B,\text{cal}}}, \quad (7)$$

that can generally result in a large overall uncertainty for the measurement. This is because even with high statistics determinations of the positions of the D1 transitions, the uncertainty in equation (7) is generally dominated by the uncertainty of the absolute calibration. The latter can have a statistical component that can be reduced by collecting more calibration data, but can also have a systematic one that is mainly due to the fact that the overall calibration function is only an approximation and
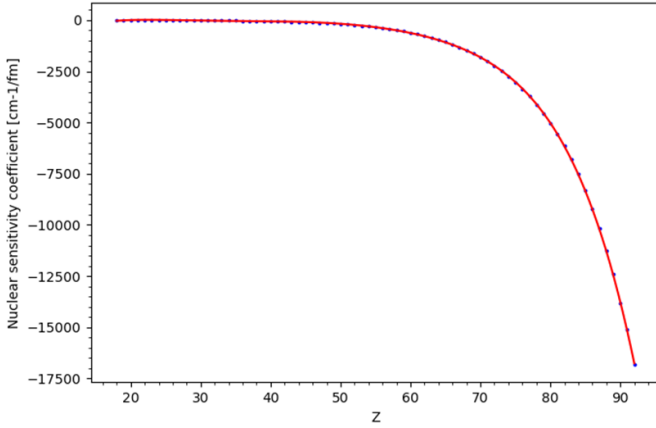
Figure 5. Nuclear sensitivity coefficients, *S*, over the Na-like isoelectronic sequence taken from [23] fitted with a polynomial for estimation. Coefficients found through least-squares minimization can be found in equation (10).

generally covers a large energy range. The systematic component of the calibration uncertainty is difficult to reduce and therefore in most cases limits the overall uncertainty of the measurement.

At small separations therefore it might be beneficial to determine the energy difference directly from many independent measurements of the separation itself as $E_{AB}^M = (E_B - E_A)^M$. In this case the pixel separation on the CCD chip can be directly turned into an energy separation using the dispersion function. The dispersion function, which is the first derivative of the calibration function, has a smaller systematic component as it expresses the local variation of the calibration as opposed to representing the full energy range measured.

$$\Delta E_{AB}^M = \sqrt{\Delta (E_A - E_B)_{\text{stat}}^2 + \Delta E_{AB,\text{Cal}}^2}. \qquad (8)$$

For larger D1 energy separations, when the lines originate from different elements that might not even be neighbors in *Z*, the uncertainty determined from the local dispersion function accumulates over the distance of the lines and becomes comparable or larger than the systematic uncertainty in the absolute separation measurement of equation (7). The term $\Delta (E_A - E_B)$ is the residual statistical distribution of the measured lines over time, which is equivalent to the instrumental resolution once systematic time drifts are corrected.

As customary [51], in count rate limited measurements the statistical uncertainty of a line position determination can be estimated from the count rate, $\dot{N}$, of the transition and the data acquisition time, *t*, as

$$\Delta E = \frac{\sigma}{\sqrt{\dot{N}t}}, \qquad (9)$$

where σ is the half-width of the spectral line. Knowing the estimated count rates allows for determining the time required to take D1 and calibration spectra.
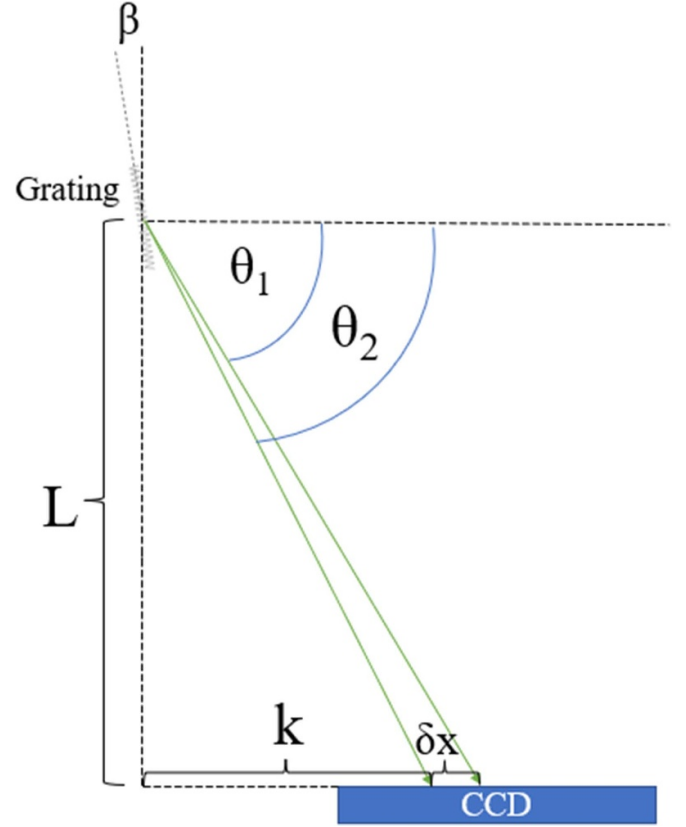

Figure 6. Generalized diffraction spectroscopic setup, used to parameterize predicted pixel separation of Na-like D1 transitions between two elements. All units are assumed to be in SI units.

A.2. Formula for the approximate scaling of the nuclear sensitivity coefficient with Z

Nuclear sensitivity coefficients have been calculated in [23] over the full Na-like isoelectronic sequence. In some cases, experimental design can benefit from a simple *Z* atomic number scaling of the coefficients that are represented in blue dots on figure 5. We found that a polynomial function can be used to approximate such a scaling, with parameters included in equation (10).

$$S(Z) = -5160 + 818Z - 51.3Z^2 + 1.64Z^3 - 2.83 \times 10^{-2}Z^4$$
$$+ 2.54 \times 10^{-4}Z^5 - 9.44 \times 10^{-7}Z^6 \ (\text{cm}^{-1}/\text{fm}). \qquad (10)$$

A.3. Estimating the pixel separation of the measured D1 lines for optical system design

Application of the general diffraction grating equation one can parameterize the linear separation, *x*, between the Na-like D1 lines on the CCD detector surface of the EUV spectrometer. Figure 6 shows the parameters that characterize the dimensions of the setup. These include the β incident angle of the incoming rays, the *L* perpendicular distance between the grating and the CCD, the *d* diffraction groove spacing (in nm/groove), and *m* the diffraction order. The

J. Phys. B: At. Mol. Opt. Phys. **57** (2024) 195001

A Hosier *et al*

$\lambda(Z)$ atomic number dependent wavelength of the Na-like D1 lines can be approximated by a polynomial whose coefficients can be determined from a least-squares fit of the transition wavelengths calculated from the energies listed in [23].

$$\lambda(Z) = -5.29 + \frac{1072}{Z} - \frac{12050}{Z^2} + \frac{315000}{Z^3} \quad [\text{nm}]. \quad (11)$$

With these the general diffraction equation is given as

$$d(\sin(\theta) - \sin(\beta)) = m\lambda. \quad (12)$$

The angle of diffraction θ can be solved simply by

$$\theta = \arcsin\left(\sin(\beta) - \frac{m\lambda(Z)}{d}\right) \quad [\text{degrees}]. \quad (13)$$

Using basic trigonometry and applying the law of cosines, one can solve for the distance, δx, (in meters) the two Na-like D1 lines of interest will have on the CCD plane. The separation in pixels can be achieved by properly converting the distance using the dimensions of the pixel.

$$\delta x(L, \beta, m, d, Z) = \frac{L}{\sin(\theta_1)\sin(\theta_2)}$$
$$\times \sqrt{\sin^2(\theta_2) + \sin^2(\theta_1) - 2\sin(\theta_1)\sin(\theta_2)\sin(\theta_2 - \theta_1)} \quad [\text{m}]. \quad (14)$$

ORCID iDs

A Hosier https://orcid.org/0000-0003-2836-6605
Dipti https://orcid.org/0000-0001-6675-8509
R Silwal https://orcid.org/0000-0003-4175-4135
G Gwinner https://orcid.org/0000-0002-6744-4365
Yu Ralchenko https://orcid.org/0000-0003-0083-9554

References

[1] Wansbeek L W, Sahoo B K, Timmermans R G E, Jungmann K, Das B P and Mukherjee D 2008 Analysis of parity nonconservation in the Ra+-Ion (arXiv:0807.1636)
[2] Gwinner G and Orozco L A 2022 Studies of the weak interaction in atomic systems: towards measurements of atomic parity non-conservation in francium *Quantum Sci. Technol.* **7** 024001
[3] Mané E *et al* 2011 *Phys. Rev. Lett.* **107** 212502
[4] Angeli I and Marinova K P 2013 table of experimental nuclear ground state charge radii: an update *At. Data Nucl. Data Tables* **99** 69–95
[5] Akylas V R and Vogel P 1978 Muonic atom cascade program *Comput. Phys. Commun.* **15** 291–302
[6] Fricke G, Bernhardt C, Heilig K, Schaller L A, Schellenberg L, Shera E B and Dejager C W 1995 Nuclear ground state charge radii from electromagnetic interactions *At. Data Nucl. Data Tables* **60** 177
[7] Knecht A Skawran A and Vogiatzi S M 2020 Study of nuclear properties with muonic atoms *Eur. Phys. J. Plus* **135** 777
[8] Gao H and Vanderhaeghen M 2022 The proton charge radius *Rev. Mod. Phys.* **94** 015002
[9] Hofstadter R, Fechter H R and McIntyre J A 1953 High-energy electron scattering and nuclear structure determinations *Phys. Rev.* **92** 978–87
[10] Nörtershäuser W and Moore I D 2022 Nuclear charge radii *Handbook of Nuclear Physics* (Springer) pp 1–70
[11] De Vries H, De Jager C W and De Vries C 1987 Nuclear charge-density-distribution parameters from elastic electron scattering *At. Data Nucl. Data Tables* **36** 495–536
[12] Chesler R B and Boehm F 1968 Isotope shifts of K X rays and variations of nuclear charge radii *Phys. Rev.* **166** 1206–12
[13] Adamczak A *et al* 2023 Muonic atom spectroscopy with microgram target material *Eur. Phys. J.* A **59** 15
[14] Vogiatzi S 2023 Studies of muonic $^{185,187}Re$, ^{226}Ra, and ^{248}Cm for the extraction of nuclear charge radii, 29082 [MSc Physics, ETH Zürich]
[15] Tsukada K *et al* 2019 Electron scattering from 208Pb and 132Xe ions at the SCRIT facility *Hyperfine Interact.* **240** 102
[16] Heilig K 1987 Nuclear charge radii from optical spectroscopy *Hyperfine Interact.* **38** 803–16
[17] Campbell P, Moore I D and Pearson M R 2016 Laser spectroscopy for nuclear structure physics *Prog. Part. Nucl. Phys.* **86** 127–80
[18] Lowe J A, Chantler C T and Grant I P 2013 Self-energy screening approximations in multi-electron atoms *Radiat. Phys. Chem.* **85** 118–23
[19] Soria Orts R *et al* 2007 Zeeman splitting and g factor of the 1 s 2 2 s 2 2 p P 3 2 2 and P 1 2 2 Levels in Ar 13+ *Phys. Rev.* A **76** 052501
[20] Elliott S R, Beiersdorfer P, Chen M H, Decaux V and Knapp D A 1998 Measurements of the differences in the nuclear charge radii among uranium isotopes *Phys. Rev.* C **57** 583–9
[21] Schuch R, Lindroth E, Madzunkov S, Fogle M, Mohamed T and Indelicato P 2005 Dielectronic resonance method for measuring isotope shifts *Phys. Rev. Lett.* **95** 183003
[22] Brandau C *et al* 2008 Isotope shift in the dielectronic recombination of three-electron ^{A}Nd^{57+} *Phys. Rev. Lett.* **100** 073201
[23] Gillaspy J D, Osin D, Yu. Ralchenko J R and Blundell S A 2013 Transition energies of the D lines in Na-like ions *Phys. Rev.* A **87** 062503
[24] Sapirstein J and Cheng K T 2011 S -Matrix calculations of energy levels of the Lithium Isoelectronic sequence *Phys. Rev.* A **83** 012504
[25] Erickson G W 1977 Energy levels of one-electron atoms *J. Phys. Chem. Ref. Data* **6** 831–70
[26] Lotz W 1970 Electron-impact ionization cross-sections for atoms up to Z = 108 *Z. Phys.* **232** 101–7
[27] Silwal R *et al* 2018 Measuring the difference in nuclear charge radius of Xe isotopes by EUV spectroscopy of highly charged Na-like ions *Phys. Rev.* A **98** 052502
[28] Silwal R *et al* 2020 Determination of the isotopic change in nuclear charge radius from extreme-ultraviolet spectroscopy of highly charged ions of Xe *Phys. Rev.* A **101** 062512
[29] Indelicato P and Desclaux J P 1990 Multiconfiguration Dirac-Fock calculations of transition energies with qed corrections in three-electron ions *Phys. Rev.* A **42** 5139–49
[30] Eides M I, Grotch H and Shelyuto V A 2001 Theory of light hydrogenlike atoms *Phys. Rep.* **342** 63–261
[31] Johnson W R, Blundell S A and Sapirstein J 1988 Many-body perturbation-theory calculations of energy levels along the sodium isoelectronic sequence *Phys. Rev.* A **38** 2699–706
[32] Blundell S 1993 Calculations of the screened self-energy and vacuum polarization in Li-like, Na-like and Cu-like ions *Phys. Rev.* A **47** 1790–803

J. Phys. B: At. Mol. Opt. Phys. **57** (2024) 195001

A Hosier *et al*

[33] Froese C F, Gaigalas G, Jönsson P and Bieroń J 2019 GRASP2018-A fortran 95 version of the general relativistic atomic structure package *Comput. Phys. Commun.* **237** 184–7

[34] Sapirstein J and Cheng K T 2015 S -matrix calculations of energy levels of sodium like ions *Phys. Rev.* A **91** 062508

[35] Coursey J S, Schwab D J, Tsai J J and Dragoset R A 2015 *Atomic weights and isotopic compositions* (Version 4.1) National Institute of Standards and Technology (available at: http://physics.nist.gov/Comp) (Accessed 19 July 2023)

[36] Seely J F, Brown C M, Feldman U, Ekberg J O, Keane C J, MacGowan B J, Kania D R and Behring W E 1991 Wavelengths and energy levels for the Na I isoelectronic sequence Y28+ through U81+ *At. Data Nucl. Data tables* **47** 1–15

[37] Wyart J F and Group T 1985 Identification of Krypton Kr XVIII to Kr XXIX spectra excited in TFR Tokamak plasmas *Phys. Scr.* **31** 539–44

[38] Ekberg J O and Svensson L Åke 1975 Spectrum and term system of Ti XII *Phys. Scr.* **12** 116–8

[39] Kononov E Y, Ryabtsev A N and Churilov S S 1979 Spectra of sodium-like ions Cu XIX-Br XXV *Phys. Scr.* **19** 328–34

[40] Crespo López-Urrutia J R *et al* 2004 Optimization of the charge state distribution of the ion beam extracted from an EBIT by dielectronic recombination *Rev. Sci. Instrum.* **75** 1560–62

[41] Hill K W *et al* 1979 Determination of Fe charge-state distributions in the princeton large torus by bragg crystal x-ray spectroscopy *Phys. Rev.* A **19** 1770–79

[42] Levine M A, Marrs R E, Henderson J R, Knapp D A and Schneider M B 1988 The electron beam ion trap: a new instrument for atomic physics measurements *Phys. Scr.* **T22** 157–63

[43] Silwal R, Takacs E, Dreiling J M, Gillaspy J D and Ralchenko Y 2017 Identification and plasma diagnostics study of extreme ultraviolet transitions in highly charged Yttrium *Atoms* **5** 30

[44] Beiersdorfer P, Crespo López-Urrutia J R, Springer P, Utter S B and Wong K L 1999 Spectroscopy in the extreme ultraviolet on an electron beam ion trap *Rev. Sci. Instrum.* **70** 276–9

[45] Fu Y, Yao K, Wei B, Lu D, Hutton R and Zou Y 2010 Overview of the shanghai EBIT *J. Instrum.* **5** C08011

[46] Blagojević B *et al* 2005 A high efficiency ultrahigh vacuum compatible flat field spectrometer for extreme ultraviolet wavelengths *Rev. Sci. Instrum.* **76** 083102

[47] Fahy K *et al* 2004 UTA versus line emission for EUVL: studies on Xenon emission at the NIST EBIT *J. Phys. D: Appl. Phys.* **37** 3225–32

[48] Draganić I N *et al* 2011 EUV spectral lines of highly-charged Hf, Ta and Au ions observed with an electron beam ion trap *J. Phys. B: At. Mol. Opt. Phys.* **44** 025001

[49] Podpaly Y A, Gillaspy J D, Reader J and Ralchenko Y 2015 Measurements and identifications of extreme ultraviolet spectra of highly-charged Sm and Er *J. Phys. B: At. Mol. Opt. Phys.* **48** 025002

[50] Blundell S A, Baird P E G, Palmer C W P, Stacey D N and Woodgate G K 1987 A reformulation of the theory of field isotope shift in atoms *J. Phys. B: At. Mol. Phys.* **20** 3663–81

[51] Hughes I and Hase T 2010 *Measurements and Their Uncertainties: A Practical Guide to Modern Error Analysis* (Oxford University Press)